AIAA SciTech Forum
7-11 January 2019, San Diego, California
AIAA Scitech 2019 Forum

10.2514/6.2019-0472

Numerical Prediction of Aero-Optical Distortions by Transonic Flow over a Cylindrical Turret

Mohammed S. Kamel*
ANSYS, Inc., Lebanon, New Hampshire 03766
Kan Wang† and Meng Wang‡
University of Notre Dame, Notre Dame, Indiana 46556

Aero-optical distortions induced by shock-boundary layer interaction over a cylindrical turret at transonic flow speeds are predicted using large-eddy simulation (LES) with wall-modeling. The flow configuration in the experiment of Vorobiev et al. (AIAA Paper 2014-2357) is considered in this study. The numerical results are validated against the steady and unsteady pressure measurements on the turret surface and the wind-tunnel wall. The aero-optical predictions are compared to the two-dimensional Shack-Hartmann wavefront data. The LES captures the low-frequency oscillations of the shock wave as it interacts with the separated shear layer and the wake. Phase averaging based on the fundamental frequency of the shock wandering motion is employed to investigate the periodic features of the flow field and optical distortions, and it is found that the piston and tilt components of the optical distortions are highly correlated with the shock-induced pressure oscillations.

Downloaded by Mohammed Kamel on March 17, 2019 | http://arc.aiaa.org | DOI: 10.2514/6.2019-0472

I. Introduction

Aero-optics is concerned with the aberration effects on a laser beam caused by the density fluctuations in compressible turbulent flows adjacent to an optical aperture.[1–4] When a collimated optical wavefront travels through a variable density field, different parts of the beams propagate at different local speeds, leading to phase distortions, which can cause beam defocus, jitter, and a dramatic reduction in the effective range of an optical system.

Turrets are widely used to point and steer the laser beam in various applications of airborne laser systems for communication, targeting, imaging and directed energy systems. A series of in-flight experiments were conducted in recent years to investigate the aero-optical environment around a hemisphere-on-cylinder turret in the Airborne Aero-Optics Laboratory-Transonic (AAOL-T) program.[5] A range of subsonic and transonic Mach numbers between 0.5 and 0.8[6,7] were tested. At $M_\infty = 0.8$, an unsteady shock is formed on top of the turret and oscillates at a dimensionless frequency of $St_D = 0.15$, which is the same as the frequency of the separation line movement. This lock-in phenomenon between the unsteady shock and the separated shear layer was also observed in wind-tunnel tests by Gordeyev et al.[8] and Vorobiev et al.[9] involving transonic flow over a cylindrical turret mounted between two flat plates of different altitudes. They found that the turret-surface pressure, the unsteady shock and the separated shear layer exhibit periodic oscillations, and as a result, the induced optical distortions oscillate at the same frequency, which is inversely proportional to the inflow Mach number.

With the rapid development of high-fidelity simulation techniques and the growth in computer power, large-eddy simulation (LES) has become an effective prediction tool for computational aero-optics.[10] However, for aero-optical applications involving wall-bounded flows, wall-resolved LES is limited to relatively low to intermediate Reynolds numbers[10–13] due to its high computational cost. Hybrid approaches combining LES with a Reynolds-averaged Navier-Stokes (RANS) method provide a more affordable alternative.

*Software Developer II at ANSYS, Inc.; formerly Research Assistant at University of Notre Dame, Department of Aerospace and Mechanical Engineering; mohammed.kamel@ansys.com; Member AIAA.
†Research Assistant Professor, Department of Aerospace and Mechanical Engineering; kwang2@nd.edu.
‡Professor, Department of Aerospace and Mechanical Engineering; m.wang@nd.edu; Associate Fellow AIAA.

Copyright © 2019 by Mohammed Kamel, Kan Wang and Meng Wang. Published by the American Institute of Aeronautics and Astronautics, Inc., with permission.

Downloaded by Mohammed Kamel on March 17, 2019 | http://arc.aiaa.org | DOI: 10.2514/6.2019-0472

Detached-eddy simulation (DES) and its variants gained popularity in the last two decades, and they were applied to simulate the aero-optical flow over the hemisphere-on-cylinder turret as in the experiment conducted by Gordeyev et al.[14] These simulations were able to capture some of the global flow features such as the mean surface pressure and wake profiles at some locations, but overall, the agreement with experimental data is not satisfactory in terms of both flow and optical results.[15–18]

Another class of hybrid LES/RANS methods is wall-modeled LES,[19,20] which computes most of the boundary layer with LES and uses a RANS type model in the near-wall region. Compared to DES, wall-modeled LES is more accurate and robust but computationally more expensive. Mathews et al.[21] recently employed wall-modeled LES to compute subsonic flow over the aforementioned hemisphere-on-cylinder turret.[14] Their results provided aero-optical predictions closest to the experimental measurements at high Reynolds numbers. Wall-modeled LES was also utilized by Kamel et al.[22] to simulate subsonic and supersonic turbulent boundary layers and subsonic separated flows over a cylindrical turret at practical Reynolds numbers. Their flow and aero-optical predictions agreed well with experimental measurements[23,24] and with results from previous wall-resolved LES at reduced Reynolds numbers.[10,13] These recent results have demonstrated the feasibility of using wall-modeled LES as a cost-effective simulation tool for aero-optical flows at realistic flow conditions.

In the present work, wall-modeled LES is employed to investigate the aero-optical distortions induced by a transonic flow over a cylindrical turret with a conformal window, as in the experiment of Vorobiev et al.[9] The emphasis is on capturing the effect of low-frequency shock-separation oscillations. A systematic procedure is followed to ensure that the numerical simulation is conducted at the experimental conditions for a choked flow case with strong shock oscillations. The relation between optical distortions and the shock oscillation above the optical aperture is investigated.

II. Computational Methodology

A compressible unstructured-mesh LES code, CharLES, developed by Cascade Technologies Inc.[25] is employed to simulate the flow field. It uses a hybrid Central-ENO finite-volume scheme to simulate flows involving shocks. A second-order central scheme blended with minimal upwinding is used in smooth flow regions, and a second-order ENO scheme is employed for shock capturing. A modified form of Ducros shock sensor[26] proposed by Bhagatwala and Lele[27] is adopted to switch the convective flux reconstruction from central scheme to ENO scheme when a shock is detected. The explicit third order Runge-Kutta method is employed for time advancement. The Vreman model is used to model the effects of sub-grid scale motions.[28,29]

To alleviate the mesh resolution requirement, an equilibrium stress-balance wall model[30] is used to provide approximate wall boundary conditions to the LES in terms of wall shear stress τ_w and heat flux q_w. The wall-model equations are solved on a secondary wall-layer mesh with an adequate resolution in the wall-normal direction. The computational expenses are significantly reduced because the LES grid scales with the outer scale of the boundary layer, which is relatively insensitive to the Reynolds number.

For optical calculations, a beam grid of the same resolution as the LES mesh is constructed along the optical beam path. The instantaneous density field is interpolated from the LES grid onto the beam grid using a second-order gradient based method. The fluctuating index of refraction n is calculated using the Gladstone-Dale relation,

$$n = 1 + K_{GD}\rho, \tag{1}$$

where K_{GD} is the Gladstone-Dale coefficient which is weakly dependent on the optical wavelength. The phase of the optical wavefront can be described by the optical path length (OPL),

$$\mathrm{OPL}(x', z', t) = \int_0^L n(x', y', z', t)dy', \tag{2}$$

where x' and z' are the local coordinates in the aperture plane and y' is the coordinate along the beam path. The phase distortions are represented by the relative difference in OPL in the plane normal to the beam path, which is called the optical path difference (OPD),

$$\mathrm{OPD}(x', z', t) = \mathrm{OPL}(x', z', t) - \langle \mathrm{OPL}(x', z', t) \rangle, \tag{3}$$

where the angle brackets indicate spatial averaging over the plane. The tip/tilt-removed OPD is calculated

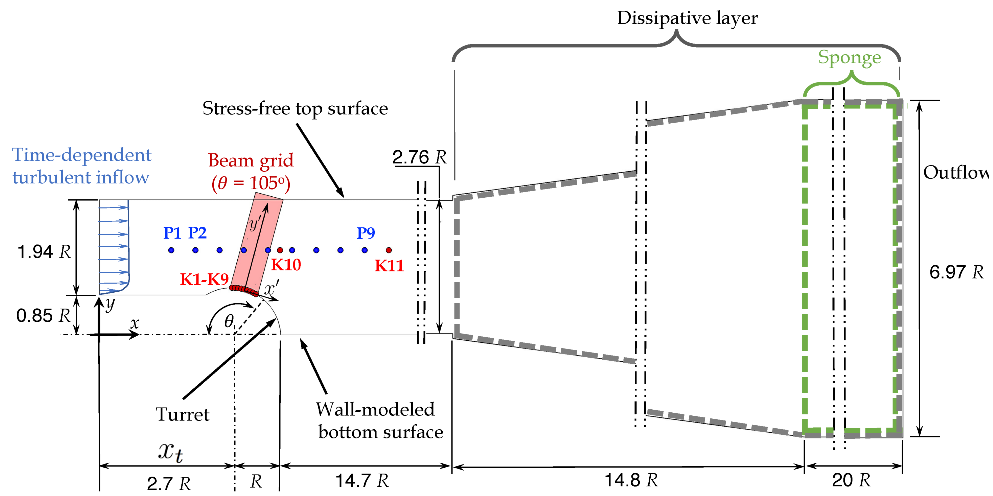

Figure 1: Computational setup for the transonic flow over a cylindrical turret.

by removing the spatially-linear components from OPL along with its spatial mean,

$$\mathrm{OPD}(x', z', t) = \mathrm{OPL}(x', z', t) - \left[C_x(t)x' + C_z(t)z' + C_o(t)\right], \tag{4}$$

where $C_x(t)$ and $C_z(t)$ are the instantaneous tilt and tip components in the x' and z' directions, respectively, and $C_o(t)$ is the spatial mean of OPL, or piston component. They are calculated using a least-square method by minimizing the function

$$G = \iint \left\{\mathrm{OPL}(x', z', t) - \left[C_x(t)x' + C_z(t)z' + C_o(t)\right]\right\}^2 dx'dz'. \tag{5}$$

III. Flow Configuration and Simulation Set-Up

The computational setup, shown schematically in Figure 1, is based on the experimental configuration of Vorobiev et al.[9] A partially-protruding cylinder with a conformal window is mounted on two flat plates with different altitudes. In the experiment two vacuum pumps were used with different valve settings to control the outlet back pressure, and consequently the incoming flow speed. Nine static pressure ports, marked P1 to P9, were placed on the side wall of the test section along with two Kulite unsteady pressure ports K10 and K11. Nine Kulite unsteady pressure sensors, K1 to K9, were distributed on the turret surface with angular steps of 3.67° in a range from −14.67° to 14.67° from the aperture center. The beam elevation angle θ is measured from the upstream direction and is equal to 105° at the aperture center. The flow field surrounding the turret surface was recorded by a high-speed shadowgraph system, which was synchronized with the unsteady pressure measurements and wavefront measurements using a high-speed 2-D Shack-Hartmann sensor. In the numerical simulation, time histories of flow variables are collected at the P and K probe locations as in the experiment. By reducing the outlet back pressure, the inflow Mach number is increased. Six different test cases, numbered from 1 to 6 in the order of decreasing back pressure, were recorded and measured in the experiment. The experimental test case 4 is considered in the numerical simulations, because it has well-defined inlet boundary conditions represented by choked inflow at inflow Mach number $M_{\infty,in} = 0.68$, and it is one of the cases characterized by strong shock oscillations.

The size of the computational domain is $53.2R$, $6.97R$ and $0.2R$, where R is the turret radius, in the streamwise, vertical and spanwise directions, respectively. Since the spanwise domain size is constant in the LES, whereas in the experiment the diffuser is three-dimensional, the slope of the diffuser walls in the simulation is increased such that the expansion rate of the cross sectional area is the same as in the experimental diffuser. The computational grid consists of 34 million points. There are 64 equally-spaced points along the span with $\Delta z = 3.125 \times 10^{-3}R$. At the inlet, the mesh spacings are $\Delta x = 0.1\delta_{in}$ and $\Delta y_{min} = 0.75 \times 10^{-2}\delta_{in}$ in the streamwise and wall-normal directions, respectively, where $\delta_{in} = 0.065R$ is the thickness of incoming turbulent boundary layer. The mesh resolution over the optical aperture is

Downloaded by Mohammed Kamel on March 17, 2019 | http://arc.aiaa.org | DOI: 10.2514/6.2019-0472

Downloaded by Mohammed Kamel on March 17, 2019 | http://arc.aiaa.org | DOI: 10.2514/6.2019-0472

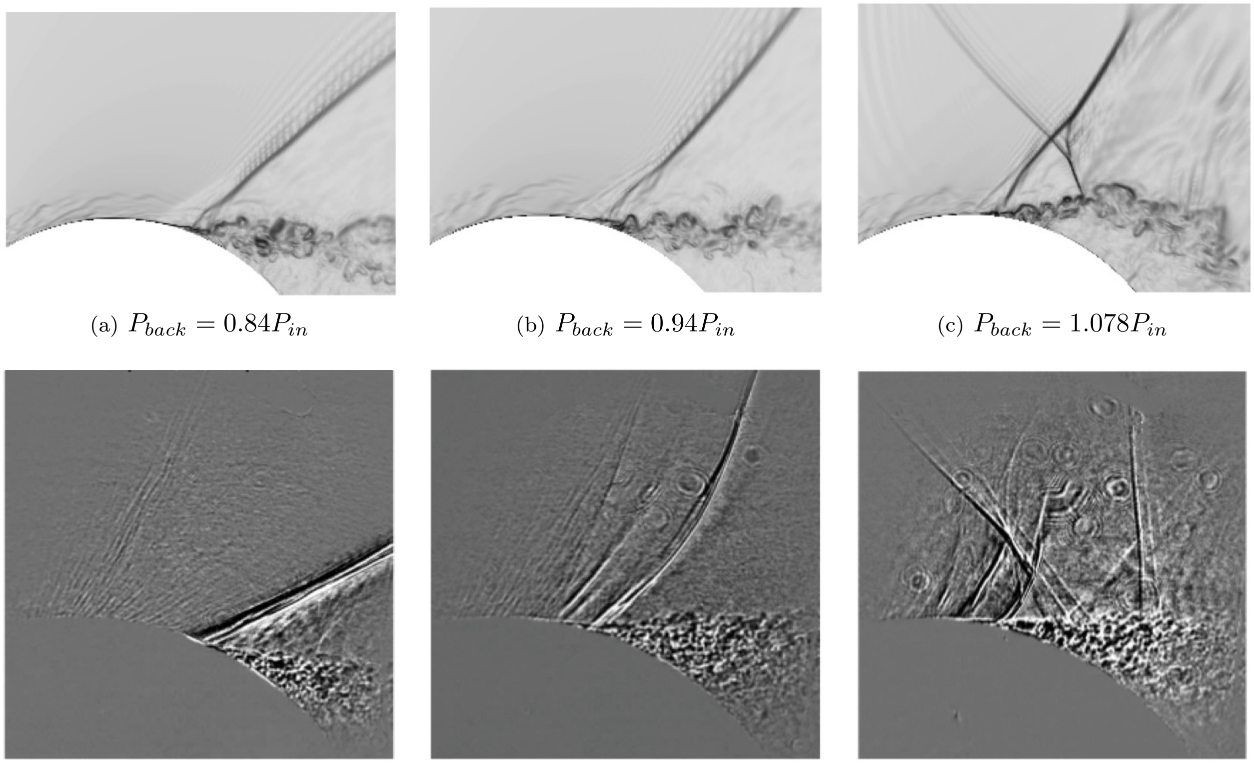

(a) $P_{back} = 0.84P_{in}$ (b) $P_{back} = 0.94P_{in}$ (c) $P_{back} = 1.078P_{in}$

(d) Minimum back pressure (e) Test case 6 (f) Test case 4

Figure 2: Qualitative comparison between numerical schlieren (a,b and c) and experimental shadowgraphs (d,e and f) of Vorobiev et al.[9]

$\Delta x = 2.5 \times 10^{-3}R$ in the streamwise direction and $\Delta y_{min} = 5 \times 10^{-4}R$ in the wall-normal direction for $\theta = 90°$ to $120°$. The mesh topology is divided into a number of grid blocks, most of which are structured and consist only of hexahedra. Only two blocks located downstream of and above the turret mesh block consist of a combination of hexahedra and prisms to ensure good mesh quality in the regions of interest.

Due to lack of experimental measurements of pressure far downstream of the turret, the back pressure assigned to the outlet is determined by an iterative procedure to match, in the least square sense, the mean pressure at the K-probes on the turret surface in experimental case 4. The flow fields corresponding to back pressures of $0.84P_{in}$, $0.94P_{in}$ and $1.078P_{in}$, where P_{in} is the static pressure at the inlet, are shown in Figures 2(a), (b) and (c), respectively, using the numerical schlieren (NS) defined as

$$\text{NS} = -10 \exp\left(\frac{\|\nabla\rho\| - \|\nabla\rho\|_{min}}{\|\nabla\rho\|_{max} - \|\nabla\rho\|_{min}}\right). \tag{6}$$

Strong shock oscillations are observed as the back pressure increases, which is consistent with experimental shadowgraphs displayed in Figures 2(d), (e) and (f). After iterations, the back pressure for the outlet boundary is set to be $P_{back} = 1.078P_{in}$, which gives the best possible match of the mean pressure on the turret surface and wind-tunnel wall as shown in Figure 3. Due to the positive mass flow rate imposed at the inlet, there is no global flow reversal even though the outlet back pressure is slightly higher than the inlet pressure.

Periodic boundary conditions are applied in the spanwise direction. Time-dependent equilibrium boundary-layer inflow at $M_{\infty,in} = 0.68$ and $Re_{\theta,in} = 1.0 \times 10^4$, where θ is the momentum thickness, is generated by an independent simulation using wall-modeled LES with the rescale and recycle technique.[31,32] The van Driest transformed mean velocity profile of the inflow is depicted in Figure 4. The bottom wall and turret surface are wall-modeled with adiabatic boundary conditions. The wall-layer thickness adjacent to the turret surface is $2.5 \times 10^{-3}R$ and contains 5 LES mesh points in the wall-normal direction. The top boundary is assigned to be impermeable and stress-free in order to minimize the mesh resolution requirement in the

Downloaded by Mohammed Kamel on March 17, 2019 | http://arc.aiaa.org | DOI: 10.2514/6.2019-0472

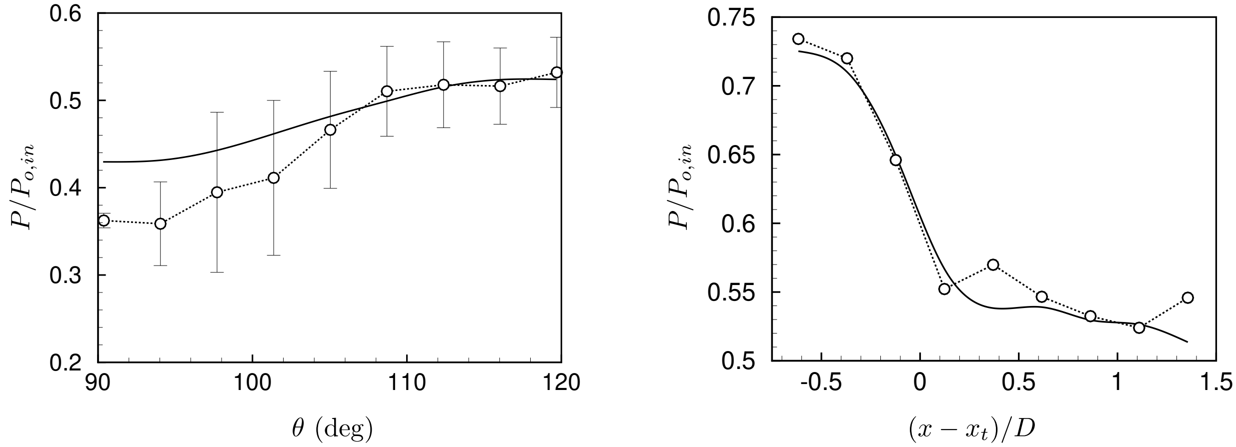

(a) Turret surface

(b) Wind-tunnel wall

Figure 3: Mean pressure distributions on the turret surface and the tunnel wall: ——, numerical predictions; - ○ -, experimental measurements of Vorobiev et al.[9]

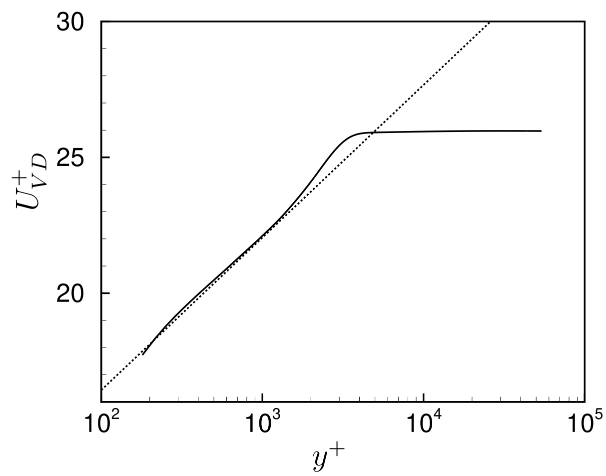

Figure 4: Mean streamwise velocity at the simulation inlet: ——, inflow generated by wall-modeled LES at $M_\infty = 0.68, Re_\theta = 1.0 \times 10^4$; - - - , logarithmic law $U^+ = (1/0.41)\ln y^+ + 5.2$.

top region, which is of less interest compared to the regions near the bottom wall and turret surface. The flow is computed using the fully-upwind dissipative scheme from $x = 15.7R$ downstream the turret axle to the outlet boundary to damp out the vortical structures and acoustic waves before the outlet boundary. In addition, the outlet boundary is preceded by a sponge layer with a thickness of $20R$.

IV. Results and Discussions

A. Flow Field

The most prominent characteristic of the flow is the strong cyclic motion of a shock wave with a time period of $t_{cycle} \approx 2.3D/U_{\infty,in}$, where D is the turret diameter. Figure 5 displays the instantaneous flowfield at different time instants during one cycle. The shock location is identified by the iso-surface of a strong negative dilatation of value $\nabla \cdot \mathbf{u} = -90a_{\infty,in}/R$, where $a_{\infty,in}$ is the inlet freestream sound speed. The vortical structures are represented by iso-surfaces of λ_2 criterion colored by streamwise velocity contours. The numerical schlieren, as defined by Eq. (6), is displayed in a spanwise plane in the back.

A strong shock induces flow separation immediately after the shock. During the upstroke, when the

Downloaded by Mohammed Kamel on March 17, 2019 | http://arc.aiaa.org | DOI: 10.2514/6.2019-0472

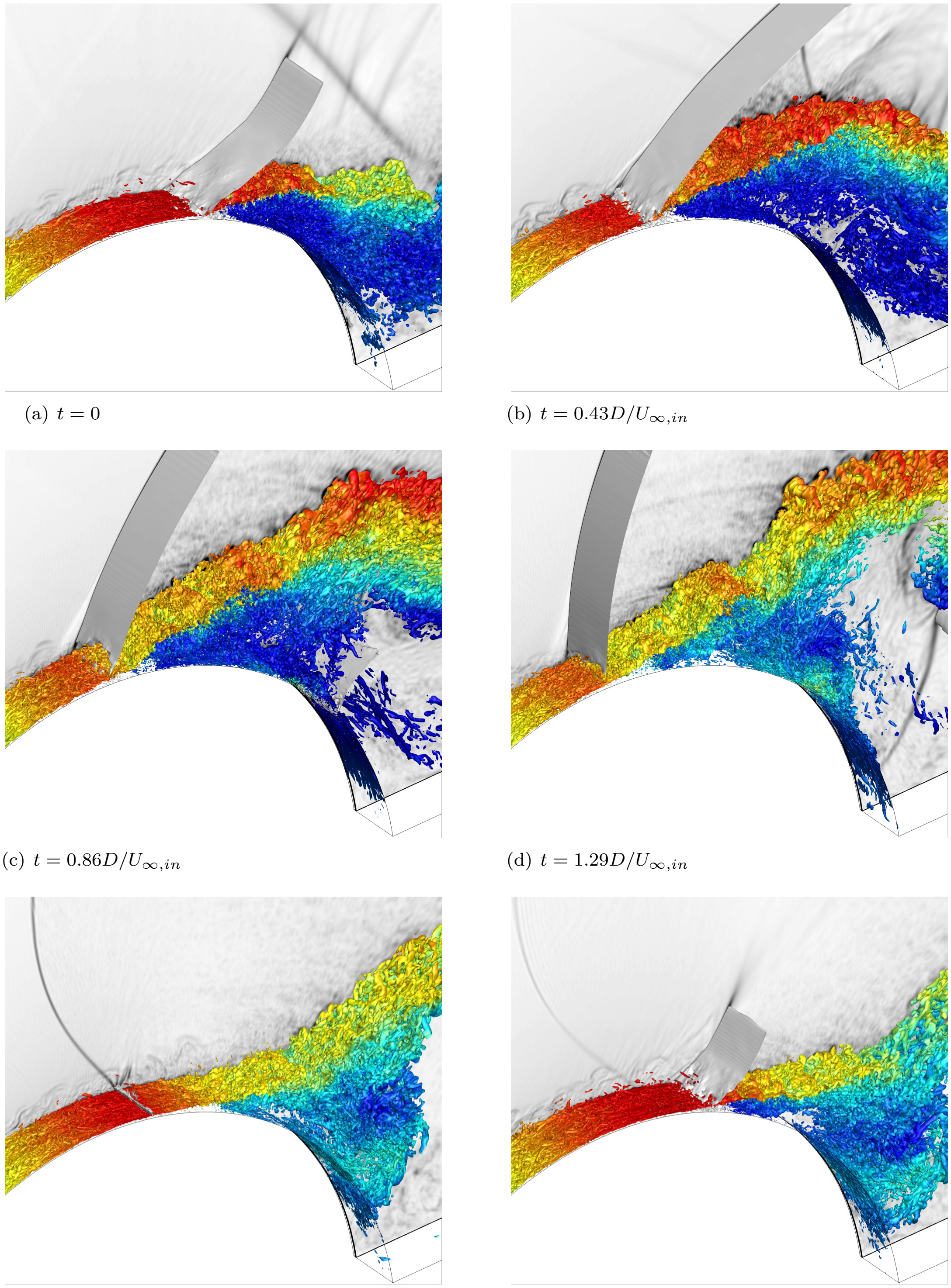

(a) $t = 0$

(b) $t = 0.43D/U_{\infty,in}$

(c) $t = 0.86D/U_{\infty,in}$

(d) $t = 1.29D/U_{\infty,in}$

(e) $t = 1.89D/U_{\infty,in}$

(f) $t = 2.15D/U_{\infty,in}$

Figure 5: Transonic flow over a cylindrical turret at six time instants. Shown in each plot are iso-surfaces of λ_2 criterion colored by the streamwise velocity, a grey iso-surface of negative dilatation indicating the shock locus, and contours of numerical schlieren in a spanwise plane in the back.

Downloaded by Mohammed Kamel on March 17, 2019 | http://arc.aiaa.org | DOI: 10.2514/6.2019-0472

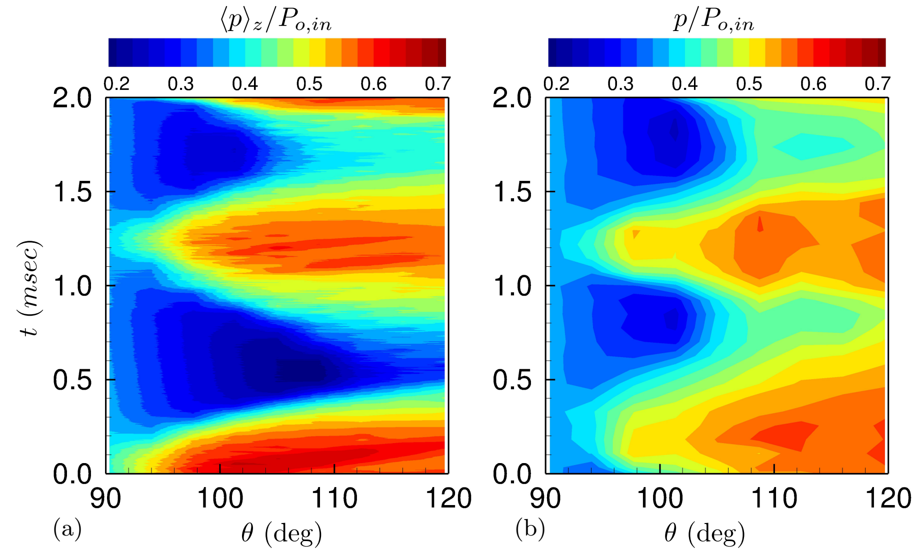

Figure 6: Instantaneous pressure on the turret surface: (a) spanwise-averaged pressure from numerical simulation; (b) experimental measurements by Kulite probes K1 to K9 (Vorobiev et al.[9]).

shock moves upstream, the separated region grows while the shock becomes weaker (Figure 5(a–e)). During the downstroke, the flow separation is reduced and the shock strengthens as it moves downstream, as shown in Figure 5(f). The shock motion and its intensity have asymmetric patterns during its upstroke and downstroke. The predicted large-scale shock oscillations are consistent with the "transonic resonance" observed by Vorobiev et al.[9] in their case 4. The three-dimensional flow visualizations in Figures 5(a-f) illustrate a strong coupling between the shock and flow separation, which resembles the shock/boundary-layer interactions observed by Johnson and Papamoschou[33] in a set of experiments of over-expanded flow inside a 2-D divergent nozzle.

At the probe locations shown in Figure 1, the flow variables are collected over a time period $T_{\text{stats}} = 43D/U_{\infty,in}$ at every 10 LES time steps, corresponding to a sampling frequency of 2.7 MHz, which is much higher than the sampling frequency of the Kulite measurements (54 kHz).[9] From Figure 5 it is observed that the key features of shock and shock-induced flow separation are highly coherent in the spanwise direction. Figure 6(a) depicts the spanwise-averaged instantaneous pressure on the turret surface at a range of elevation angles from 90° to 120° covering the optical aperture. These computed values are compared to the experimental measurements by Kulite probes K1 to K9 as shown in Figure 6(b). The pressure in both figures is normalized by the inlet total pressure $P_{o,in}$. The predicted unsteady pressure exhibits low-frequency oscillations at approximately 1 kHz ($St_D = fD/U_{\infty,in} = 0.426$) due to the shock wandering, which is consistent with the experimental observations. However, the levels of the pressure fluctuations are overpredicted compared to the experimental measurements.

B. Aero-Optical Predictions

The beam grid over the region $L_{x'} \times L_{y'} \times L_{z'} = 0.583R \times 2.02R \times 0.2R$ has 7.67×10^6 grid points in total, with 235 points in the x'–direction. In comparison, the Shack-Hartmann wavefront sensor employed in the experiment has 60 subapertures in the same direction.

The optical results are calculated over a time period $T_{\text{stats}} = 18D/U_{\infty,in}$. The density field is collected every 10 time steps, corresponding to a sampling frequency of 2.7 MHz, whereas the sampling frequency of the 2-D wavefront sensor is 13.5 kHz. When the beam grid points are located outside the computational domain, the density is set to the free-stream value. The effect of this approximation is included in the steady lensing term, which is the time-averaged wavefront distortion and is removed before studying optical distortions.

Figures 7(a), (b) and (c) display the time histories of piston, tilt and tip components of the optical distortions, respectively, compared to the pressure fluctuations, $p'/P_{o,in}$, at the aperture center ($\theta = 105°$).

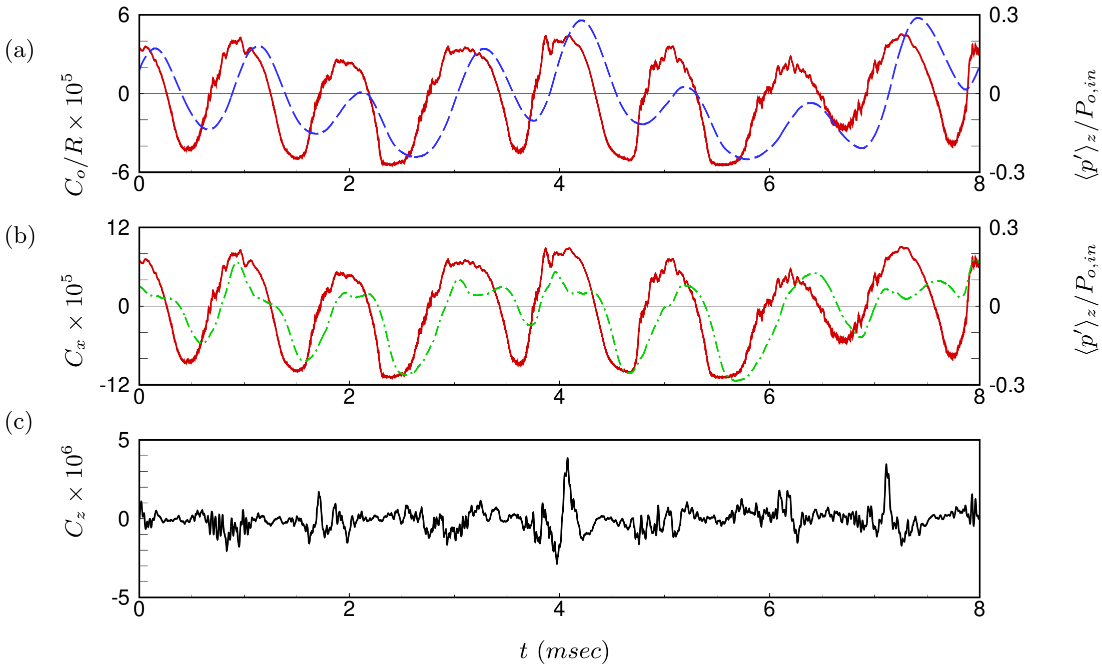

Figure 7: Instantaneous optical wavefront components and spanwise-averaged pressure fluctuations at the aperture center: – – –, piston (C_o/R); – · –, tilt (C_x); ——, tip (C_z); ——, spanwise avgeraged pressure fluctuations ($\langle p' \rangle_z / P_{o,in}$).

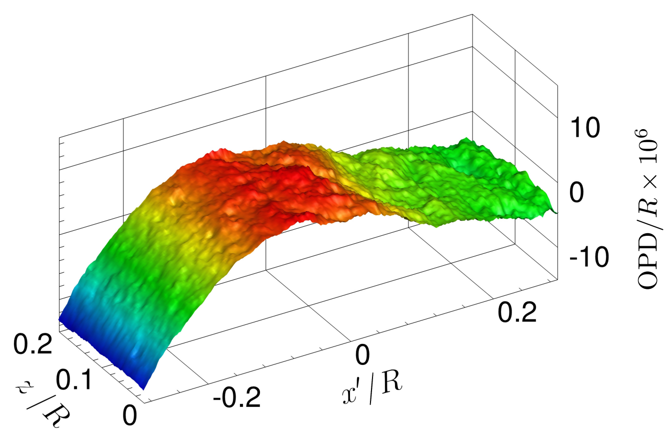

Figure 8: Instantaneous piston- and tip/tilt-removed OPD.

The piston and tilt components are highly correlated with turret-surface pressure fluctuations, and both are strongly affected by the shock wandering. On the other hand, the spanwise tip component is an order of magnitude smaller than the streamwise tilt component and has no significant low-frequency content.

Figure 8 depicts an instantaneous OPD field after removing piston and tip/tilt components. It shows that the spanwise variation of wavefront distortions is relatively small. Therefore the OPD is spanwise-averaged hereafter to focus on its variation in the streamwise direction. Figures 9(a) and (b) show the time-variation of the instantaneous spanwise-averaged OPD from the numerical simulation and experimental measurements, respectively. Similar patterns are observed. The footprint of the periodic shock motion over the aperture is clearly indicated by the discontinuities in the wavefront, which is more pronounced during the downstroke and weaker during the upstroke.

Downloaded by Mohammed Kamel on March 17, 2019 | http://arc.aiaa.org | DOI: 10.2514/6.2019-0472

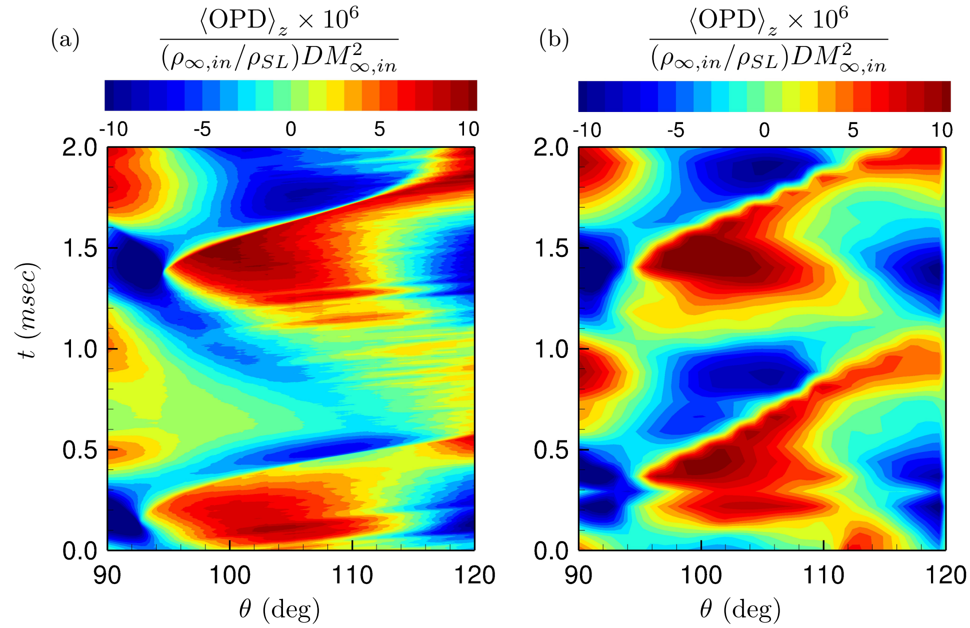

Figure 9: Instantaneous piston-tip-tilt-removed spanwise-averaged OPD: (a) numerical prediction; (b) experimental measurements (Vorobiev et al.[9]).

C. Flow and Aero-Optical Analysis Using Phase Averaging

Based on the fundamental frequency of the shock motion, phase averaging is applied on a number of flow and optical quantities to analyze the periodic flow features and the associated aero-optical distortions. The phase- and spanwise-averaged pressure fluctuations at each of the K-probe locations from K1 to K9 are cross-correlated with a reference sinusoidal function of the same fundamental frequency to determine the phase difference $\Delta\phi$ between the two signals. Then, the mean phase delay, $\Delta\phi_{\mathrm{mean}}$, is calculated as an average over these cross-correlations. The phases are corrected for all phase-averaged flow and optical quantities based on the calculated value of $\Delta\phi_{\mathrm{mean}}$.

The phase-averaged piston and tilt components of optical distortions are plotted in Figure 10 along with the phase-averaged turret-surface pressure at the aperture center (i.e., $\theta = 105°$). The piston and tilt components are highly correlated with the surface pressure. The phase-averaged piston has a phase shift of $\Delta\phi = 60°$ with respect to the phase-averaged pressure fluctuations at the aperture center. The positive peak of the tilt occurs at the same phase of $\phi \simeq 90°$ as the peak pressure signal, whereas its negative peak shows a phase delay of $\Delta\phi = 30°$ from the negative peak of the pressure fluctuations.

Figures 11(a) and (b) show the iso-contours of the phase- and spanwise-averaged OPD as a function of elevation and phase angles from the numerical simulation and experimental measurements, respectively. Although they show very similar wavefront structures, the magnitude of optical distortions from the LES is lower than that from the experiment. The footprint of the shock oscillations above the aperture is evident in both plots.

V. Conclusion

Transonic flow over a cylindrical turret is computed using wall-modeled LES under the same flow conditions as in test case 4 in the experiment of Vorobiev et al.[9] In this test case, the flow is choked inside the test section, and the inflow is at $M_{\infty,in} = 0.68$ and $Re_{\theta,in} = 10^4$. The back pressure is determined via an iterative procedure to provide a best match with the mean pressure on the turret surface. The low-frequency shock oscillation is well-predicted by the numerical simulation, and its fundamental frequency, $fD/U_{\infty,in} = 0.426$, agrees with the experimental measurements. However, the magnitude of pressure fluctuations is overpredicted. It is shown that the optical distortions are mainly caused by the low-frequency periodic motion of the shock over the optical aperture and shock induced separation. The piston and streamwise tilt compo-

Downloaded by Mohammed Kamel on March 17, 2019 | http://arc.aiaa.org | DOI: 10.2514/6.2019-0472

Downloaded by Mohammed Kamel on March 17, 2019 | http://arc.aiaa.org | DOI: 10.2514/6.2019-0472

nents of the wavefront distortions are highly correlated with the aperture-surface pressure fluctuations. The patterns of wavefront distortions are consistent with the 2-D wavefront measurements in the experiment. Phase averaging is applied on the flow and optical quantities based on the fundamental frequency of the shock motion, and the results demonstrate the dominant effect of the wandering shock on the piston, tilt and high-order components of wavefront distortions.

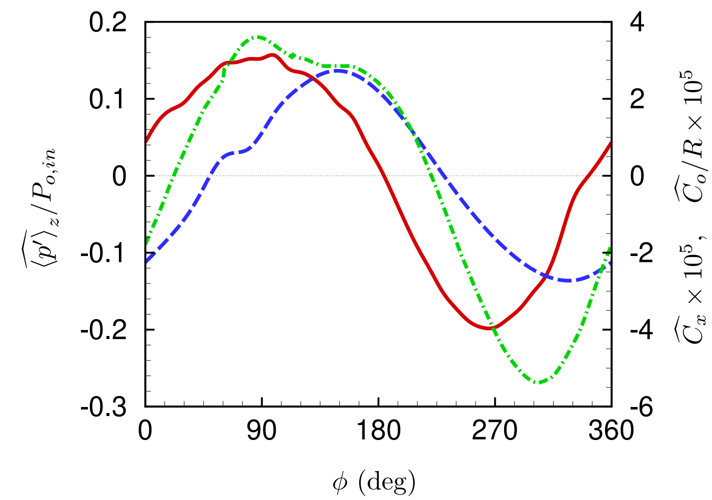

Figure 10: Phase-averaged pressure and aero-optical quantities: – – –, piston (C_o/R); – · –, tilt (C_x); ——, pressure fluctuations at the aperture center.

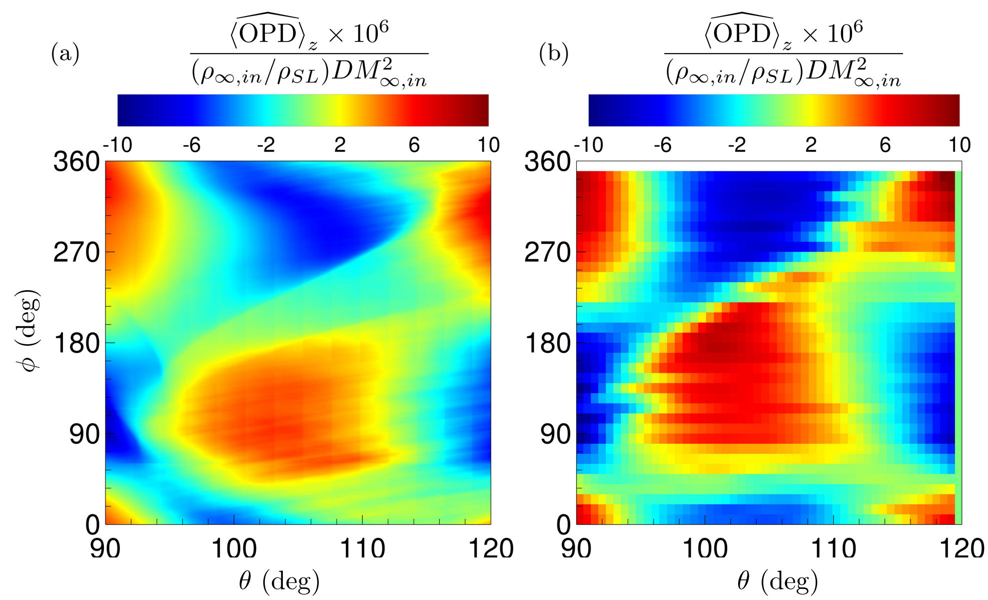

Figure 11: Normalized phase- and spanwise-averaged OPD: (a) numerical prediction; (b) experimental measurements (Vorobiev et al.[9]).

Downloaded by Mohammed Kamel on March 17, 2019 | http://arc.aiaa.org | DOI: 10.2514/6.2019-0472

Acknowledgments

The work presented in this paper is part of the Ph.D. dissertation research of Mohammed Kamel at the University of Notre Dame.[34] This research has been supported by the High Energy Laser Joint Technology Office (HEL-JTO) through AFSOR Grant FA950-13-1-0001. Computational resources were provided by the University of Notre Dame Center of Research Computing and an NSF Extreme Science and Engineering Discovery Environment (XSEDE) research allocation through Grant ACI-1548562. The authors acknowledge Alexander Vorobiev, Stanislav Gordeyev and Eric Jumper for providing their experimental data and helpful discussions.

References

[1]Gilbert, K. G. and Otten, L. J., *Aero-Optical Phenomena, Progress in Astronautics and Aeronautics*, New York, AIAA, 1982.

[2]Jumper, E. J. and Fitzgerald, E. J., "Recent Advances in Aero-optics," *Progress in Aerospace Sciences*, Vol. 37, No. 3, 2001, pp. 299–339.

[3]Jumper, E. J. and Gordeyev, S., "Physics and Measurement of Aero-Optical Effects: Past and Present," *Annual Review of Fluid Mechanics*, Vol. 49, 2017, pp. 419–441.

[4]Wang, M., Mani, A., and Gordeyev, S., "Physics and Computation of Aero-Optics," *Annual Review of Fluid Mechanics*, Vol. 44, 2012, pp. 299–321.

[5]Jumper, E. J., Gordeyev, S., Cavalieri, D., Rollins, P., Whiteley, M., and Krizo, M., "Airborne Aero-Optics Laboratory-Transonic (AAOL-T)," *AIAA Paper 2015-0675*.

[6]Morrida, J. J., Gordeyev, S., and Jumper, E. J., "Transonic Flow Dynamics over a Hemisphere in Flight," *AIAA Paper 2016-1349*.

[7]Morrida, J., Gordeyev, S., Lucca, N. D., and Jumper, E. J., "Shock-Related Effects on Aero-Optical Environment for Hemisphere-on-Cylinder Turrets at Transonic Speeds," *Applied Optics*, Vol. 56, No. 16, pp. 4814–4824.

[8]Gordeyev, S., Burns, R., Jumper, E., Gogineni, S., Paul, M., and Wittich, D., "Aero-Optical Mitigation of Shocks around Turrets at Transonic Speeds Using Passive Flow Control," *AIAA Paper 2013-0717*.

[9]Vorobiev, A., Gordeyev, S., Jumper, E., Gogineni, S., Marruffo, A., and Wittich, D. J., "Low-Dimensional Dynamics and Modeling of Shock-Separation Interaction over Turrets at Transonic Speeds," *AIAA Paper 2014-2357*.

[10]Wang, K. and Wang, M., "Aero-Optics of Subsonic Turbulent Boundary Layers," *Journal of Fluid Mechanics*, Vol. 696, 2012, pp. 122–151.

[11]Mani, A., Moin, P., and Wang, M., "Computational Study of Optical Distortions by Separated Shear Layers and Turbulent Wakes," *Journal of Fluid Mechanics*, Vol. 625, 2009, pp. 273–298.

[12]Wang, K., Wang, M., Gordeyev, S., and Jumper, E., "Computation of Aero-Optical Distortions over a Cylindrical Turret with Passive Flow Control," *AIAA Paper 2010-4498*, 2010.

[13]Wang, K. and Wang, M., "Computational Analysis of Aero-Optical Distortions by Flow over a Cylindrical Turret," *AIAA Journal*, Vol. 54, No. 5, 2016, pp. 1461–1471.

[14]Gordeyev, S., Hayden, T., and Jumper, E. J., "Aero-Optical and Flow Measurements over a Flat-Windowed Turret," *AIAA Journal*, Vol. 45, No. 2, 2007, pp. 347–357.

[15]Nahrstedt, D., Hsia, Y., Jumper, E., Gordeyev, S., Ceniceros, J., Weaver, L., DeSandre, L., and McLaughlin, T., "Wind Tunnel Validation of Computational Fluid Dynamics-Based Aero-Optics Model," *Proceedings of the Institution of Mechanical Engineers, Part G: Journal of Aerospace Engineering*, Vol. 223, No. 4, 2009, pp. 393–406.

[16]Ladd, J., Mani, M., and Bower, W., "Validation of Aerodynamic and Optical Computations for the Flow about a Cylindrical/Hemispherical Turret," *AIAA Paper 2009-4118*.

[17]Morgan, P. and Visbal, M. R., "Numerical Investigation of Flow around a Turret," *AIAA Paper 2007-4480*.

[18]Morgan, P. and Visbal, M., "Hybrid RANS/LES Simulations for Flow around Two Turret Configurations," *AIAA Paper 2008-0550*.

[19]Bose, S. T. and Park, G. I., "Wall-Modeled Large-Eddy Simulation for Complex Turbulent Flows," *Annual Review of Fluid Mechanics*, Vol. 50, 2018, pp. 535–561.

[20]Piomelli, U. and Balaras, E., "Wall-Layer Models for Large-Eddy Simulations," *Annual Review of Fluid Mechanics*, Vol. 34, 2002, pp. 349–374.

[21]Mathews, E. R., Wang, K., Wang, M., and Jumper, E. J., "LES of an Aero-Optical Turret Flow at High Reynolds Number," *AIAA Paper 2016-1461*.

[22]Kamel, M. S., Wang, K., and Wang, M., "Predictions of Aero-Optical Distortions Using LES with Wall Modeling," *AIAA Paper 2016-1462*.

[23]Gordeyev, S., Cress, J., Smith, A., and Jumper, E. J., "Improvement in Optical Environment over Turrets with Flat Window Using Passive Flow Control," *AIAA Paper 2010-4492*, 2010.

[24]Gordeyev, S., Jumper, E. J., Ng, T., and Cain, A., "The optical environment of a cylindrical turret with a flat window and the impact of passive control devices," *AIAA Paper 2005-4657*, 2005.

[25]Khalighi, Y., Nichols, J. W., Lele, S., Ham, F., and Moin, P., "Unstructured Large Eddy Simulation for Prediction of Noise Issued from Turbulent Jets in Various Configurations," *AIAA Paper 2011-2886*.

[26]Ducros, F., Ferrand, V., Nicoud, F., Weber, C., Darracq, D., Gacherieu, C., and Poinsot, T., "Large-Eddy Simulation of the Shock/Turbulence Interaction," *Journal of Computational Physics*, Vol. 152, No. 2, 1999, pp. 517–549.

[27]Bhagatwala, A. and Lele, S. K., "A Modified Artificial Viscosity Approach for Compressible Turbulence Simulations," *Journal of Computational Physics*, Vol. 228, No. 14, 2009, pp. 4965–4969.

[28]Vreman, A., "An Eddy-Viscosity Subgrid-Scale Model for Turbulent Shear Flow: Algebraic Theory and Applications," *Physics of Fluids*, Vol. 16, No. 10, 2004, pp. 3670–3681.

[29]You, D. and Moin, P., "A Dynamic Global-Coefficient Subgrid-Scale Eddy-Viscosity Model for Large-Eddy Simulation in Complex Geometries," *Physics of Fluids*, Vol. 19, No. 6, 2007, 065110.

[30]Kawai, S. and Larsson, J., "Wall-Modeling in Large Eddy Simulation: Length Scales, Grid Resolution, and Accuracy," *Physics of Fluids*, Vol. 24, No. 1, 2012, 015105.

[31]Lund, T. S., Wu, X., and Squires, K. D., "Generation of turbulent Inflow Data for Spatially-Developing Boundary Layer Simulations," *Journal of Computational Physics*, Vol. 140, No. 2, 1998, pp. 233–258.

[32]Urbin, G. and Knight, D., "Large-Eddy Simulation Of A Supersonic Boundary Layer Using An Unstructured Grid," *AIAA Journal*, Vol. 39, No. 7, 2001, pp. 1288–1295.

[33]Johnson, A. D. and Papamoschou, D., "Instability of Shock-Induced Nozzle Flow Separation," *Physics of Fluids*, Vol. 22, No. 1, 2010, 016102.

[34]Kamel, M. S., *Aero-Optical Prediction of High-Reynolds Number Flows Using Wall-modeled Large-Eddy Simulation*, Ph.D. thesis, University of Notre Dame, 2017.

Downloaded by Mohammed Kamel on March 17, 2019 | http://arc.aiaa.org | DOI: 10.2514/6.2019-0472